THE JOURNAL OF PHYSICAL CHEMISTRY A

pubs.acs.org/JPCA Article

Predicting Absorption and Emission Maxima of Polycyclic Aromatic Azaborines: Reliable Transition Energies and Character

Robert W. Lamb, Alan K. Schrock, Michael T. Huggins, and Charles Edwin Webster*

Cite This: J. Phys. Chem. A 2021, 125, 3–12 Read Online

ACCESS | Metrics & More | Article Recommendations | Supporting Information

ABSTRACT: Polycyclic aromatic azaborines have potential applications as luminophores, novel fluorescent materials, organic light-emitting diodes, and fluorescent sensors. Additionally, their relative structural simplicity should allow the use of computational techniques to design and screen novel compounds in a rapid manner. Herein, the absorption and emission maxima of twelve polycyclic aromatic BN-1,2-azaborine analogues containing the N-BOH moiety were examined to determine a methodology for reliably predicting both the energy and character (local excitation [LE] vs charge transfer [CT]) of the absorption and emission maxima for these compounds. The necessity of implicit solvation models was also investigated. The cam-QTP(01) functional with a small, double-ζ quality basis set provides reliable data compared to EOM-CCSD/cc-pVDZ single-point computations. Of note, commonly used functionals for these applications (B3LYP and ωB97xD) struggle to provide reliable results for both the energy and LE character of the transitions relative to EOM-CCSD computations.

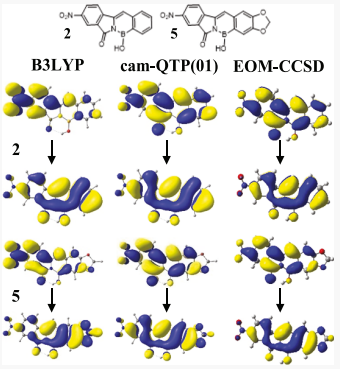

INTRODUCTION

Replacing one of the C−C groups in an aromatic benzenoid with a B−N group results in an aromatic azaborine compound. Polycyclic aromatic azaborines have been extensively studied due to their intense absorption, high quantum yields, and photostability.[1−5] Materials containing these chromo-/luminophores have potential applications in devices such as organic field effect transistors (OFETs) and organic light-emitting diodes (OLEDs).[4,6−10] Additionally, several luminescent azaborines have been reported that are relatively small, with some previously reported compounds having only three fused rings.[5,11] Due to their potential applications and their relative structural simplicity, these compounds are prime candidates for computational design and screening if a viable methodology can be determined. Based on the data in our previous publication,[11] a reasonable correlation to the experiment could be found for the predicted maxima of nearly all compounds in Figure 1 using TD-B3LYP (with a double-zeta quality basis set) single-point computations (absorption, λ_{max}) or optimizations (emission, λ_{em}) on single molecules in isolation. However, the computed data for the nitro compounds gave a poor correlation to the experimental results for λ_{em}. Experimental data suggested a possible intramolecular charge transfer (ICT) mechanism evidenced by the significant solvation dependence on λ_{em}. Drastic improvement was observed in the correlation between computed and experimental data upon utilizing a ΔSCRF (self-consistent reaction field) procedure with an external iteration (EI) state-specific solvation model. For clarification, the ΔSCRF procedure is when the ground state energy at the excited state geometry is subtracted from the energy of the excited state with the energy

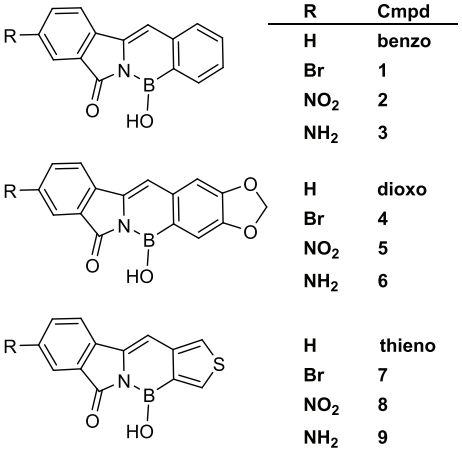

R	Cmpd
H	benzo
Br	1
NO_2	2
NH_2	3
H	dioxo
Br	4
NO_2	5
NH_2	6
H	thieno
Br	7
NO_2	8
NH_2	9

Figure 1. Polycyclic azaborines examined herein.

of both states being corrected by EI solvation. Furthermore, a negative shift in the computed Φ_S indices (a quantitative measure of spatial overlap between the attachment and detachment densities;[12] see Table S2 in the Supporting Information) of the prominent excitations supports the experimental assignment of an ICT process.

Received: June 24, 2020
Revised: December 1, 2020
Published: January 4, 2021

https://dx.doi.org/10.1021/acs.jpca.0c05765
J. Phys. Chem. A 2021, 125, 3−12

While the computed data provided a reasonable correlation to the experimental data, there is certainly room for improvement. Using the ΔSCRF procedure to correct the energies of excitations from linear response (LR) solvation is more time-intensive and does not lend itself to more black-boxed approaches for compound screening. Furthermore, due to the increased reported ICT character of both the absorption and emission processes of the nitro compounds, there could be a strong method dependence on the computed λ_{em}.[11] Indeed, previous studies have shown that standard hybrid functionals, in particular, B3LYP, can inaccurately describe long-range charge transfer processes.[13−16] Additionally, these compounds can also be construed as derivatives of cyanine dyes, for which TD-DFT almost systematically overestimates the energy of the CT state.[17] Further complicating matters, computational studies on closely related azaborine, BODIPY, and aza-BODIPY derivatives indicate that TD-DFT methods not only overestimate the energies of the vertical excitations by more than 0.3 eV on average,[18−21] but also multiple metrics indicate that CT does not play a significant role in this error.[19] Such determinations put our previous assignments of a CT-based emission in a precarious position. On one hand, the data provide a reasonable correlation and nicely corroborate experimental findings. On the other, the methodology employed has produced mixed results on systems bearing similar functional units. Herein, our prior B3LYP results are re-evaluated against additional methods to (1) definitively assign the character of the nitro emission maxima and (2) potentially establish an operationally simpler methodology for future studies.

THEORETICAL METHODS

All DFT (where DFT = B3LYP,[22,23] PBE0,[24−26] B97D,[27] cam-QTP(01),[28] LC-ωHPBE,[29] or ωB97xD[30]) computations were carried out using the D.01 revision of Gaussian 09[31] (G09) or the A.03 revision of Gaussian 16[32] (G16) as specified below. The cam-QTP(01) functional uses the cam-B3LYP framework but retunes the range separation parameters. This functional can be utilized in Gaussian by calling the cam-B3LYP functional and adjusting IOp(3/107), IOp(3/108), IOp(3/130), IOp(3/131), IOp(3/119), IOp(3/120), and IOp(3/78) to the appropriate values.[28] Default integration grids were used for all computations: G09 defaults to a fine pruned grid using 75 radial shells with 302 points per shell (75,302) for optimizations and a pruned coarse grid using 35 radial shells with 110 points per shell (35,110) for Hessians, and G16 defaults to an ultrafine pruned grid using 99 radial shells with 590 points per shell (99,590) for optimizations and a pruned SG1 grid using 50 radial shells with 194 points per shell (50,194) for Hessians. All computations with G09 used non-default (10^{-6}) SCF convergence criteria; all computations in G16 utilized default (10^{-8}) convergence criteria. All coupled-cluster computations were carried out using Q-Chem 5.0[33] using default SCF (10^{-8}) and CC (10^{-6}) convergence criteria. All DFT computations used the BS1 basis set defined as follows: the 6-31G(d′) basis sets for H, B, C, N, and O (the 6-31G(d′) basis set adopts the d polarization functions from the 6-311G(d)[34] basis set rather than the default value of 0.8[35] for B, C, N, and O) and the Hay and Wadt basis set (BS) and effective core potential (ECP) [LANL2DZ][36] combination with d and p polarization functions developed by Gilbert and Sunderlin et al. [LANL2DZ(d,p)][37] for Br and S, when present. All coupled-cluster computations used the BS2 basis set defined as follows: the cc-pVDZ basis set for H, B, N, C, O, and S, when present, and the aug-cc-pVDZ-PP BS+ECP combination[38] for Br, when present. All DFT single-point computations for determining pK_as were performed on the B3LYP/BS1 geometries using the linear response SMD[39] solvation model with parameters consistent with acetonitrile as the solvent and the BS3 basis set defined as follows: the cc-pVTZ[40] basis sets for all atoms and additional diffuse functions placed on the two O atoms involved in the hydrogen bonding to the acidic proton (jul-cc-pVTZ).[41] All ground state geometries were fully optimized in G09 with DFT/BS1, and subsequent analytical frequency computations confirmed that a zeroth-order saddle point was obtained. For time-dependent DFT (TD-DFT) geometry optimizations, the first singlet excited states were optimized in G09 using analytical gradients, and the first 10 singlet excitations were solved iteratively [TD(ROOT = 1,NSTATES = 10)]. Subsequent single-point frequency computations were performed on the TD-DFT optimized geometries in G16 to employ analytical Hessians (G09 has only numerical Hessians for TD-DFT) and confirmed that in each case, a zeroth-order saddle point was obtained. To simulate the absorption and emission spectra with TD-DFT, single-point computations were performed on the optimized ground state (GS) and excited state (ES) geometries, and the first 30 singlet excitations were solved iteratively [TD(ROOT = 1,NSTATES = 30)]. To simulate the spectra with EOM-CCSD/BS2, single-point computations were performed on the corresponding B3LYP/BS1 (absorption) and TD-B3LYP/BS1 (emission) geometries, and the first 20 singlet excitations were solved iteratively. All spectra were simulated using an in-house Fortran program by convoluting the computed excitation energies and oscillator strengths with a Gaussian line shape and a broadening of 20 nm.[42] DFT and EOM-CCSD computations were performed both on single molecules in isolation ("gas-phase") and with the SMD solvation model using parameters consistent with either chloroform or acetonitrile as the solvent.[39] These implicit solvation models employed either the linear response (LR) or the state-specific external iteration (EI)[43,44] formalisms as noted below. Emission 0-0 energies were also attempted via the Franck−Condon−Herzberg−Teller (FCHT) approach using the S_0 and S_1 analytical vibrational frequencies (for these purposes only, the S_0 frequencies were recomputed as single-point computations in G16).[45−48] However, "poor progression" for several compounds precluded a rigorous analysis across all methodologies. The data from FCHT computations with B3LYP/BS1 and cam-QTP(01)/BS1 are discussed in the Supporting Information. Attachment and detachment densities and their corresponding Φ_S (spatial overlap) values were obtained using the Nancy_Ex code.[12,49,50] Natural transition orbitals were also generated for the transitions corresponding to λ_{max} or λ_{em} in the simulated spectra to examine the character of the transitions and the images rendered in Chemcraft[51] with a contour value of 0.02.

RESULTS AND DISCUSSION

"Gas-Phase" Computations. In accordance with Head-Gordon et al.'s observations,[13] a series of long-range-corrected functionals were selected to compute λ_{max} and λ_{em} and compared to their non-range-corrected counterparts. In an effort to simplify computational procedures, initial computations were performed without a solvation model ("gas-phase") and compared to the experimental results in $CHCl_3$, the least

https://dx.doi.org/10.1021/acs.jpca.0c05765
J. Phys. Chem. A 2021, 125, 3−12

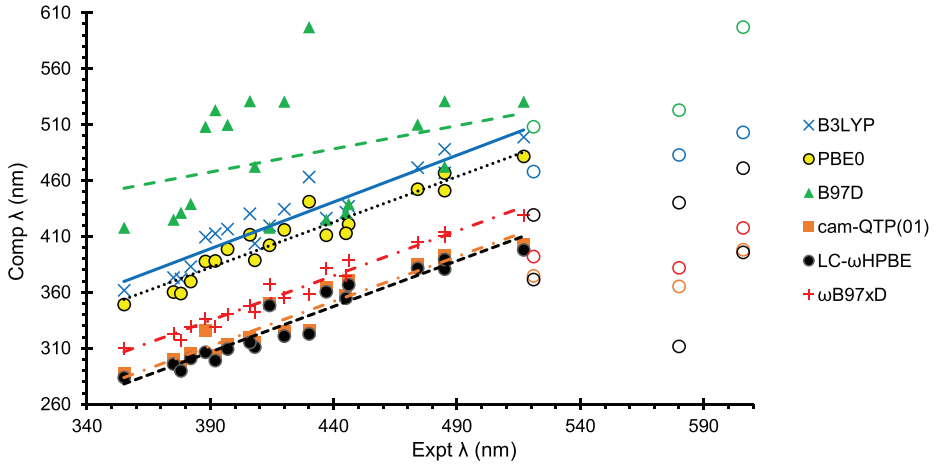

Figure 2. Computed λ_{max} (TD-DFT//DFT/BS1) and λ_{em} (TD-DFT/BS1) vs experimental data in $CHCl_3$. The colored circles denote the λ_{em} from the nitro compounds (see the online version for the colors).

polar solvent utilized in the experimental studies. Figure 2 shows that among the non-range-corrected functionals, the hybrids (B3LYP and PBE0) produce a better correlation to experimental data than the pure B97D functional based on the scatter of each data series from its trend line. Each range-corrected functional produces a series with significantly less scatter compared to its non-range-corrected counterpart, indicating a more reliable correlation compared to experimental data. However, the hybrid functionals also produce three apparent outliers to the data, each of which corresponds to the λ_{em} of the nitro compounds (colored circles in Figure 2). Additionally, the displacement of the nitro λ_{em} from the remainder of the computed appears to be exaggerated with the range-corrected functionals. This trend would indicate that the range-corrected functionals overestimate the energy (lower wavelength) of the experimentally assigned charge transfer emission, a behavior that would not be surprising given that these are "gas-phase" computations.

Before delving too deeply into methodological differences, the "right" answer (in terms of the trends from a benchmark methodology) should be established. Therefore, EOM-CCSD/BS2 single-point computations were performed on the B3LYP/BS1 geometries (EOM-CCSD/BS2//B3LYP/BS1). Nevertheless, one point to consider quite carefully is the expense of EOM-CCSD computations on systems of this size. What if the EOM-CCSD computations, however unlikely, also do not reproduce experimental data? Another more tractable method would be needed that could provide data of similar quality. To this end, results from the cam-QTP(01) functional as a more affordable alternative were compared to experimental and EOM-CCSD results (this DFT functional "looks like the right" answer for an "okay" reason). Moreover, this functional was explicitly developed to predict more accurate ionization energies, which require accurate computation of orbital energies.[28] In a similar vein, the orbital energies from cam-QTP(01) should lend themselves to more accurate excitation energies. Indeed, in its original publication, cam-QTP(01)/aug-cc-pVTZ was shown to provide results comparable to coupled-cluster methods for a fraction of the computational expense.[28] However, due to the size of the molecules of interest in the current study, the BS1 basis set was used in place of the much larger aug-cc-pVTZ with cam-QTP(01) computations. At an intermediate cost, CIS(D)/BS2//B3LYP/BS1 computations were also explored and are documented in the Supporting Information.

Figure 3 shows the results of EOM-CCSD and cam-QTP(01) compared to experimental data in $CHCl_3$. As

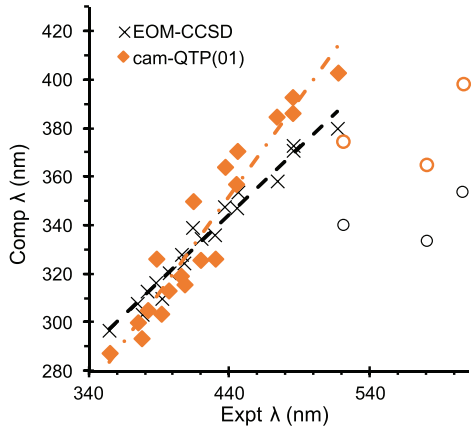

Figure 3. Computed λ_{max} and λ_{em} from EOM-CCSD/BS2//B3LYP/BS1 and cam-QTP(01)/BS1 vs experimental data in $CHCl_3$. The colored circles denote the λ_{em} from the nitro compounds.

postulated, the computed excitations from cam-QTP(01) are in quite reasonable agreement with EOM-CCSD, albeit with a slightly different slope (subsequent computations with cam-QTP(01)/aug-cc-pVTZ//cam-QTP(01)/BS1 are also qualitatively similar, see the Supporting Information). Unfortunately, despite the generally excellent correlation for the rest of the data, EOM-CCSD does not predict λ_{em} for the nitro compounds that are in agreement with the experimental data. Recalling that the data in Figure 3 represents "gas-phase" computations and the predicted character from B3LYP and the experiment is an ICT transition,[11] this observation is not necessarily shocking. However, across the results for each range-corrected functional and EOM-CCSD, the λ_{em} of the nitro compounds is consistently further away from the trend line compared to standard hybrid functionals. One would expect that range-corrected functionals would predict a higher energy for CT transitions compared to non-range-corrected functionals like B3LYP and PBE0. In a similar vein, EOM-CCSD computations have been shown to systematically overestimate the energies of some ESs.[52−54] Another possible

https://dx.doi.org/10.1021/acs.jpca.0c05765
J. Phys. Chem. A 2021, 125, 3−12

explanation is that the range-corrected functionals and EOM-CCSD do not actually predict the experimentally assigned ICT transition for the nitro λ_{em}. To investigate this possibility, the natural transition orbitals (NTOs) for the λ_{max} and λ_{em} of each compound at each level of theory were generated and compared. The full sets of orbitals for all compounds are shown in Tables S4 and S5 in the Supporting Information; a subset is shown in Figure 4.

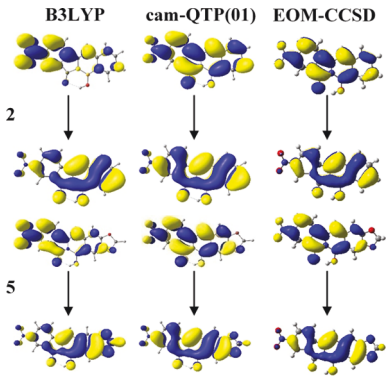

Figure 4. NTOs of λ_{em} for nitro compounds **2** and **5** at the TD-B3LYP/BS1, TD-cam-QTP(01)/BS1, and EOM-CCSD/BS2//TD-B3LYP/BS1 levels of theory. The emission process is depicted as the particle residing in the upper orbital undergoing vertical de-excitation to the lower orbital.

The NTOs in Figure 4 highlight the CT transition predicted by B3LYP for compounds **2** and **5**. Surprisingly, cam-QTP(01) and EOM-CCSD computations predict a transition that is not at all CT but rather LE in character. Moreover, each range-corrected functional predicts that the λ_{em} for the nitro compounds are LE in character and each non-range-corrected functional predicts a λ_{em} that is CT in character (Table S5). It was possible that this apparent LE character could have been a cyanine transition. However, cyanine states are often characterized by significant double-excitation character,[55] whereas all compounds in this case are definitively single-excitation character according to EOM-CCSD (Table S25). The LE character predicted by both the range-corrected functionals and EOM-CCSD is quite inconsistent with the experimental ICT assignment. In particular, the inconsistency of the transition predicted by EOM-CCSD relative to the experiment is quite disconcerting. Importantly, these are "gas-phase" computations. Perhaps, these results indicate that a solvation model is required in order to bring the nitro λ_{em} in line with the rest of the data.

Solvation Computations. Considering that the absorption maxima are consistent with the experiment across all methodologies thus far, only the emission maxima will be examined for solvent optimizations. Additionally, since the largest Stokes shifts are observed in an acetonitrile solvent (ACN), solvent optimizations were carried out with TD-DFT/BS1 and the SMD solvation model using parameters consistent with ACN (SMD-TD-DFT/BS1) (Figure 5). Because the DFT methods consistently display a different character between the range-corrected and non-range-corrected versions, we first opted to examine how the solvation scheme might impact the linear correlations (LR, EI, and ΔSCRF). These data are summarized in Figure S1 and Table S1 in the Supporting Information. Overall, the EI solvation scheme brings data from B3LYP closer to the trend line, but data with ωB97xD are essentially unchanged relative to the LR solvation scheme. These data demonstrate that the CT transition predicted by the standard hybrid functionals is indeed stabilized by the state-specific solvation scheme, whereas the LE excitation predicted by the range-corrected hybrids is not drastically impacted. A more detailed examination of the impact of the solvation scheme is provided in the Supporting Information. Ultimately, the more operationally complex EI solvation does not resolve the discrepancy between the nitro λ_{em} and the rest of the data set across methodologies. Therefore, the functionals and character will be examined using only LR solvation for the remainder of the results discussed in this contribution.

The predicted λ_{em} using an LR solvation model overall results in less scatter in the data, the most notable improvement coming from B97D. It appears that the λ_{em} of the nitro compounds is in better agreement, but in each case, extrapolating the trend line from the rest of the data shows that the energy of the λ_{em} transition is still consistently overestimated (lower wavelength) compared to the rest of the data. Continuing from before, these results should also be compared to EOM-CCSD computations. Figure 6 shows the comparison of cam-QTP(01) and EOM-CCSD computations employing

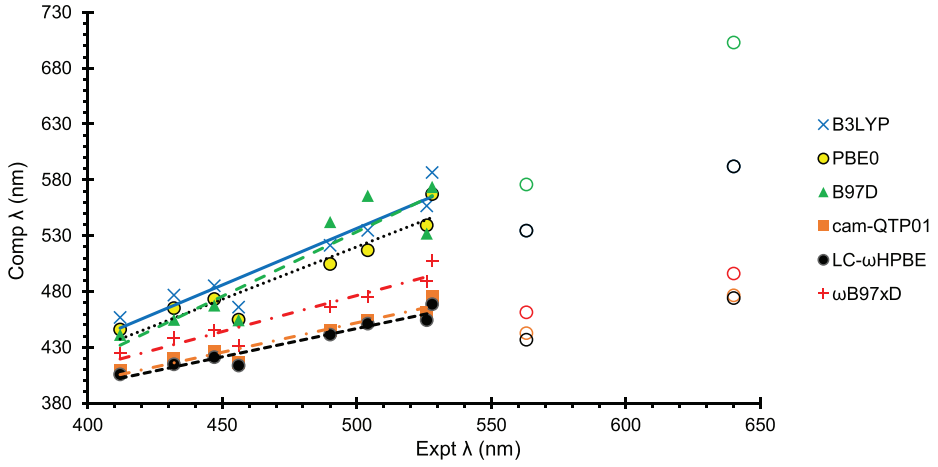

Figure 5. Computed λ_{em} (LR-SMD-TD-DFT/BS1) vs experimental data in ACN. The colored circles denote the λ_{em} from the nitro compounds (see the online version for the colors).

https://dx.doi.org/10.1021/acs.jpca.0c05765
J. Phys. Chem. A 2021, 125, 3−12

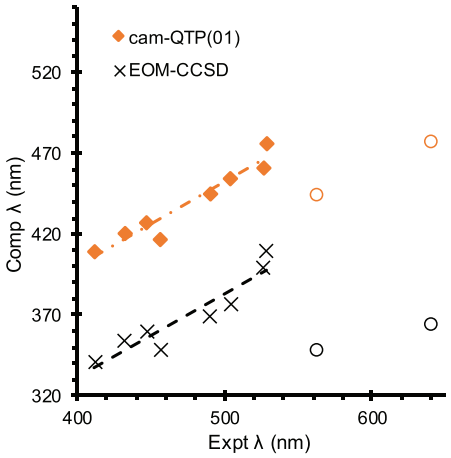

Figure 6. Computed λ_{em} from LR-SMD-EOM-CCSD/BS2//LR-SMD-TD-B3LYP/BS1 and LR-SMD-TD-cam-QTP(01)/BS1 vs experimental data in ACN. The colored circles denote the λ_{em} from the nitro compounds.

an LR solvation model. Yet again, the nitro compounds do not fall on the same line as the rest of the data. Based on the data in Figure 6, application of an LR solvation model, even with EOM-CCSD, does not rectify the discrepancy of λ_{em} from the experimental values. In fact, the EOM-CCSD results are further away from the rest of the data than any of the DFT methods, which is quite strange. However, before drawing too many conclusions, the character of the transitions should also be inspected. Without a solvation model, EOM-CCSD—and all of the range-corrected functionals—predicted that the λ_{em} of the nitro compounds was LE in character. NTOs were again generated for the λ_{em} of each compound at each level of theory. The full set of orbitals for all compounds is tabulated in Table S6 in the Supporting Information; a subset is shown in Figure 7. Based on the NTO images in Figures 4 and 7, using an LR solvation model with B3LYP, cam-QTP(01), or EOM-CCSD does not change the character of the computed emission for the nitro compounds relative to the gas-phase computations. The range-corrected functionals and EOM-CCSD still predict an LE transition, while the non-range-corrected functionals predict a CT transition.

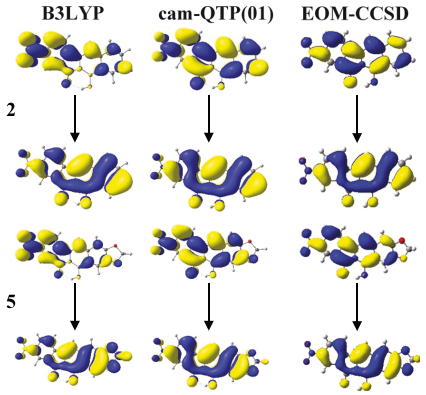

Figure 7. NTOs of λ_{em} for nitro compounds **2** and **5** at the LR-SMD-TD-B3LYP/BS1, LR-SMD-TD-cam-QTP(01)/BS1, and LR-SMD-EOM-CCSD/BS2//TD-B3LYP/BS1 levels of theory with an acetonitrile solvent. The emission process is depicted as the particle residing in the upper orbital undergoing vertical de-excitation to the lower orbital.

These observations are disconcerting; even with more rigorous methodologies, we are unable to predict a λ_{em} that has both a reasonable numerical value and CT character. The B97D functional comes quite close, but its discrepancy from EOM-CCSD computations presents a cause for caution. At this point, we must step back and re-examine the overall picture. Six DFT methods and EOM-CCSD have been pursued. The non-range-corrected functionals are the only methods that predict CT transitions for λ_{em} of the nitro compound, and still, operationally complex EI solvation schemes employed in our previous publication were required to make the transition energy better align with the experiment.[11] B3LYP has also been explicitly implicated for poor performance in predicting CT excitations. The methods anticipated to be more accurate for these applications—cam-QTP(01), LC-ωHPBE, ωB97xD, and EOM-CCSD—all predict an LE transition for the nitro λ_{em}. Based on consistent results of the range-corrected functionals with EOM-CCSD computations, the LE transition is likely the chemically correct assignment for the emission of the nitro compounds as presented. However, an LE is inconsistent with the experimentally assigned CT emission in terms of both character and wavelength. Based on these points, the ES chemistry of the nitro compounds is likely different from the −Br, −H, and $-NH_2$ analogues.

Differences in the ESs. *NTO Comparison.* To understand the differences in the ES chemistry between the nitro and non-nitro compounds, the state that is initially populated upon vertical excitation should be well-established. Due to the larger singlet-triplet gap in organic molecules and the presence of only a single conjugated π framework, the nature of the initial Franck−Condon state should be the most indicative of how the ES geometries will relax. Therefore, the character of the computed absorption maxima will be re-examined. The NTOs for the computed λ_{max} of all compounds with each method are shown in Table S4 in the Supporting Information. From these orbital images, there are no drastic differences between methods. Based on the particle orbitals from non-range-corrected functionals, upon excitation, the electron density is more localized toward the $-NO_2$ group in the nitro compounds. However, the range-corrected functionals and EOM-CCSD show a relatively delocalized density in the nitro compounds upon excitation, a behavior that is consistent with every other derivative. The consistent LE character of the absorption makes sense. The experimental λ_{max} are not drastically different from one another, and the computed λ_{max} have been in relatively good agreement with the experiment with all methodologies employed thus far. Because there are no drastic differences in the particle density across each compound and method, the influence of the substituents on each hole−particle pair will be examined more closely.

Both the −Br and $-NH_2$ groups act as a π donors; accordingly, there are densities present in the hole orbitals of both the Br and NH_2 compounds that are consistent with a lone pair orbital involved in an antibonding interaction with the rest of the π system. In the particle orbitals, these contributions are absent, indicating that these substituents will likely have minimal contribution to the relaxation of the geometry in the ES. As expected, the −H group has minimal contribution to both the hole and particle orbitals and effectively serves as a reference for more electron-donating/-withdrawing groups. The $-NO_2$ group contribution to the hole orbitals could be described as unexpectedly small

https://dx.doi.org/10.1021/acs.jpca.0c05765
J. Phys. Chem. A 2021, 125, 3−12

considering that this moiety functions as a strong π acceptor. However, the $-NO_2$ contribution to the particle orbitals is significantly greater. In fact, the $-NO_2$ groups consistently have a greater contribution to the particle orbitals than the hole orbitals, indicating that these groups will impact how the ES geometry relaxes.

ES Resonance Structures of Nitro Compounds. Based on the particle NTOs, the initially populated ES for the nitro compounds can be drawn as a migration of the electron density such that both oxygen atoms of the $-NO_2$ moiety bear a formal negative charge and one of the aryl carbons becomes a carbocation (Scheme 1). From this structure, multiple

Scheme 1. Reorganization of the Electron Density upon Excitation, Based on the Computed NTOs, and Resonance Structures Thereof

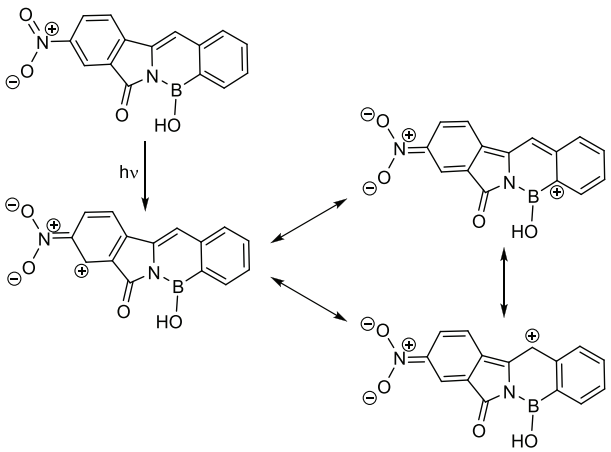

resonance forms can be drawn that place the carbocation within the azaborine ring. The delocalization of a positive charge in this manner is not accessible with the other derivatives and could be the cause of the difference in their ES properties. By placing a positive charge within the azaborine ring, electron density can be pulled away from neighboring groups, one of which is the NBOH moiety, in particular, the $-OH$ group, which would make the proton more acidic. Photoacids are not a novel concept, particularly for cyanine derivatives;[56] their presence in azaborine compounds has been less studied.

GS vs ES Acidity. The pK_a of the GS and ES for each compound can be computed and compared to determine if the nitro compounds truly are more acidic in the ES than the GS as a result of the resonance forms shown in Scheme 1. Since the equilibrium constant is related to the free energy of reaction (eq 1), the pK_as can be calculated with the following equations by computing the free energy for loss of a proton from each compound (eq 2).

$$\Delta G_{rxn} = -RT \ln(K) \quad (1)$$

$$\Delta G_{rxn} = [G_{proton} + G_{anion}] - G_{neutral} \quad (2)$$

We recognize that accurately determining the pK_a of a compound from computed thermodynamic data is quite challenging. Here instead, we focus on the change in pK_a between the GS and the ES. Once the pK_a of both the GS and ES geometries have been determined, the difference between these values (ΔpK_a) can be used to evaluate whether a compound becomes more, or less, acidic in the ES. The only thing necessary at this point is a method for reliably calculating the ΔG_{rxn} for the deprotonation reaction. To that end, we use a slightly modified version of the methodology described in the Jaguar manual.[57] This methodology employs optimizations at the B3LYP/6-31G(d) level of theory with subsequent single-point computations at the B3LYP/(aug)-cc-pVTZ level theory where the diffuse functions are added only to the atoms directly involved in the deprotonation reaction. Additionally, all computations employ the LR-SMD solvation model for the desired solvent. Our modifications are (1) instead of the 6-31G(d) basis set, the 6-31G(d′) basis set was employed to take advantage of the optimized d orbital coefficients for second row atoms in the geometry optimization, and (2) because we are not attempting to compare directly to the experiment but rather determine the change in the pK_a between the GS and ES geometries, we do not apply the empirical corrections and instead use the so-called "raw" pK_a for these comparisons. The ΔpK_a values for each compound are shown in Figure 8.

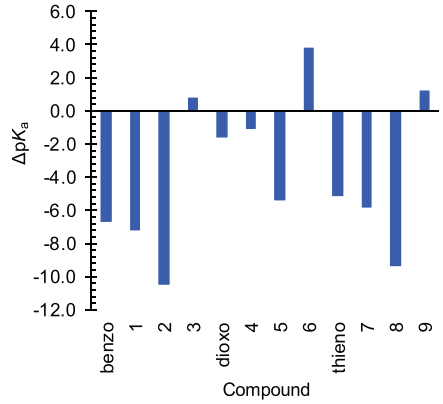

Figure 8. ΔpK_a values from LR-SMD-B3LYP/BS3//B3LYP/BS1 and LR-SMD-TD-B3LYP/BS3//TD-B3LYP/BS1.

What is immediately apparent is that most of the compounds are more acidic in the ES than the GS. Contrary to the trend, the NH_2 compounds all have a less acidic ES (positive ΔpK_a), likely due to the strong π-donation of the $-NH_2$ moiety. Furthermore, within each substituent series, benzo, dioxo, and thieno, the nitro compounds have the most negative ΔpK_a values. These data indicate that the resonance structures shown in Scheme 1, wherein the formal positive charge is positioned near the NBOH moiety, have enough contribution to the overall structure to cause a change in the behavior of the excited state relative to the compounds with π-donating substituents. Based on these data and the trends in the emission maxima from our previous publication,[11] the interaction of the solute with the solvent has an important role. Accordingly, the absolute pK_a for both the GS and ES of each compound, and thereby the ΔpK_a, is likely influenced by explicit solute−solvent interactions. Because of the difficulty in modeling explicit solute−solvent interactions, these data may not correlate precisely with the experiment (additional discussion in the Supporting Information). However, the trend in the nitro compounds relative to the others in each substituent series is difficult to ignore.

Deprotonated Nitro Compounds. Now that a plausible difference in the ES of these compounds has been established, its impact on the computed λ_{em} must be examined. Figure 9 shows the comparison of λ_{em} to the experimental values using

https://dx.doi.org/10.1021/acs.jpca.0c05765
J. Phys. Chem. A 2021, 125, 3−12

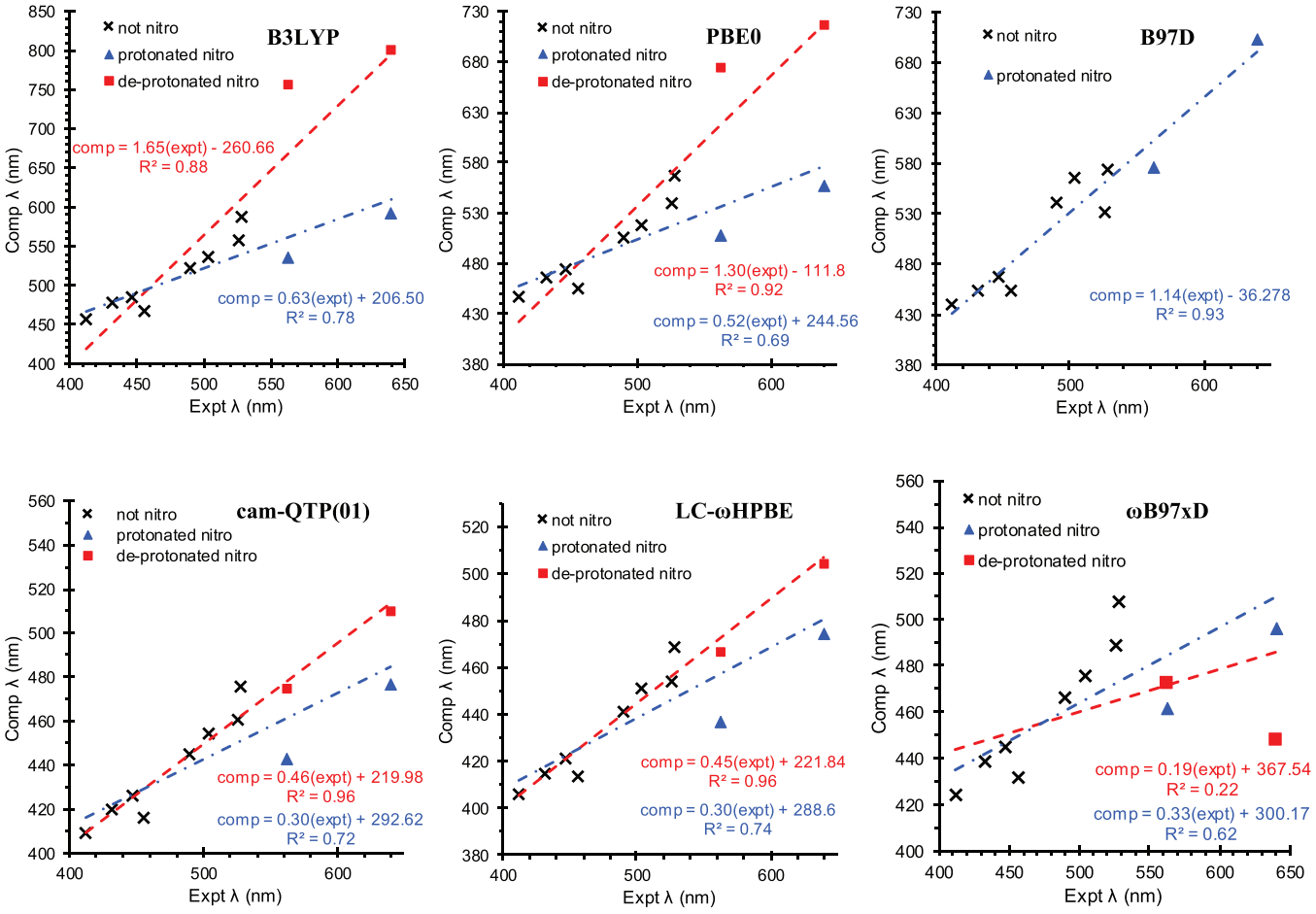

Figure 9. Computed λ_{em} from LR-SMD-TD-DFT/BS1 vs experimental data in ACN. The blue triangles denote the λ_{em} for the protonated nitro compounds, and the red squares denote the λ_{em} for the deprotonated nitro compounds. The other analogues are shown as black ×s.

either protonated or deprotonated nitro compounds determined from each DFT method. EOM-CCSD computations were not performed for the anions due to the computational expense and the fact that cam-QTP(01) has provided rather similar data thus far. The data from the non-range-corrected functionals (Figure 9, top) are somewhat mixed. Based solely on the data points, it is not readily apparent which protonation state better describes the data. However, the R^2 value indicates that the deprotonated nitro compounds have a slightly better agreement with experimental data with both B3LYP and PBE0. Unfortunately, the deprotonated nitro compounds were not located with B97D after repeated attempts. Strangely, the data from ωB97xD (Figure 9, bottom right) show an abysmal correlation with deprotonated nitro compounds, and the protonated nitro compounds have already been established as inconsistent with the experiment. The results from cam-QTP(01) and LC-ωHPBE (Figure 9, bottom left/middle) provide definitive assignments. Not only is the correlation to experimental data better with the deprotonated nitro compounds, the data points for the nitro compounds are now essentially on the trend lines. Additional range-corrected functionals available in Q-Chem (ωB97X-V, ωB97X-D3, HSE-HJS, LC-rVV10, ωB97M-V, M11, MN12-SX, and ωM06-D3) were also tested and provided similar results (Figures S5−S7 in the Supporting Information).

Using a functional that has provided results similar to EOM-CCSD computations (cam-QTP(01)), the computed λ_{em} are now in agreement with the experimental values, but do these transitions have the experimentally assigned CT character? The NTOs for the anionic nitro compounds with each DFT method are tabulated in Table S7 in the Supporting Information; a subset of the data is shown in Figure 10. The NTOs from B3LYP are relatively unchanged in character. If anything, the CT character shown in Figure 10 has become more pronounced compared to the neutral precursor (Figure 7). Similarly, the character of the NTOs for ωB97xD and cam-QTP(01) in Figure 10 is also relatively unchanged from their neutral precursors (Figure 7), although cam-QTP(01) appears to have slight changes in both the particle and hole orbitals toward CT character. Taking the cam-QTP(01) results as a reflection of the "right" answer, based on previous comparisons to EOM-CCSD, these data suggest that for the nitro compounds, the emission process itself may not be truly CT in nature. The computed Φ_S indices (degree of spatial overlap between the attachment and detachment densities of a transition) with cam-QTP(01) (Table S3) demonstrate that the emission from the nitro compounds generally has slightly more CT character than the other analogues, and the anionic nitro compounds indeed have marginally more CT character than their neutral precursors. However, these Φ_S values are still ~0.8, firmly placed within the regime of LE character.[12]

The computational data from the range-corrected functionals firmly suggest an LE emission process for the nitro compounds, which, albeit inconsistent with the initial

https://dx.doi.org/10.1021/acs.jpca.0c05765
J. Phys. Chem. A 2021, 125, 3−12

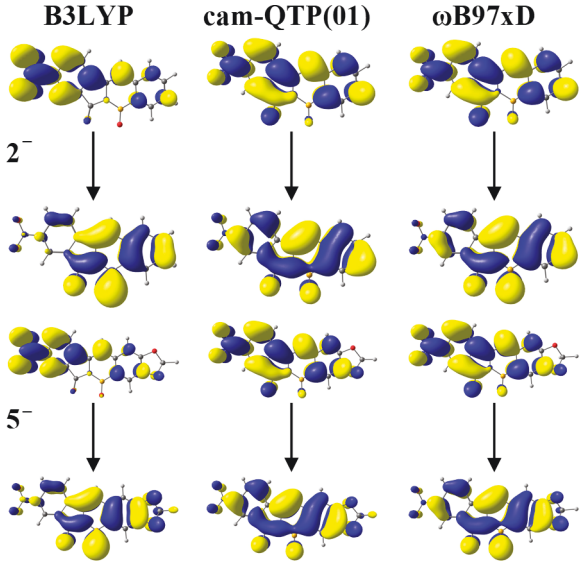

Figure 10. NTOs of λ_{em} for deprotonated nitro compounds $\mathbf{2}^-$ and $\mathbf{5}^-$ at the LR-SMD-TD-DFT/BS1 level of theory (DFT = B3LYP, cam-QTP(01), or ωB97xD) with an acetonitrile solvent. The emission process is depicted as the particle residing in the upper orbital undergoing vertical de-excitation to the lower orbital.

experimental assignment, is consistent with the behavior of all other compounds studied. Moreover, the emission λ_{em} from the anionic nitro compounds, even with LE character, is in better agreement with experimental data than the neutral nitro compounds. Taken together, these data indicate that the nitro emission likely arises from a structure resembling the deprotonated form. The word "resembling" here is important. It is possible that during relaxation of the ES, the proton is donated to a neighboring molecule that participates in H-bonding with the NBOH moiety. This would result in a structure that can be formally described as an anionic azaborine that is hydrogen-bound to a neighboring molecule. Creating a charge separation in this fashion would certainly be more stabilized in more polar solvents, thus lowering the energy of this ES and increasing λ_{em}. Unfortunately, explicit solute−solute and, more so, solute−solvent interactions are far more complicated to model correctly, particularly with DFT methods. However, given the sum total of the data presented herein, the data are most consistent with nitro compounds not displaying ICT emission but rather functioning as photoacids. By generating a formally anionic azaborine in the ES, the differential solvation (stabilization) of the negative and positive charges is responsible for the significantly larger Stokes shifts observed for the nitro compounds.

CONCLUSIONS

We have demonstrated that in agreement with previous observations, the non-range-corrected functionals do not accurately handle CT excitations. In these systems, the non-range-corrected functionals appear to overestimate the CT character of the computed transition. In the case of B97D, the wavelengths of the CT transitions are in fortuitous agreement with the experimental data, but the CT character of the transition is inconsistent with EOM-CCSD computations. The range-separated functionals provide results that are consistent with both experimental observations and EOM-CCSD computations. The authors recommend caution when comparing only numerical λ_{max} and λ_{em} to experimental values as both the wavelength and the character of the predicted transition should be in agreement with experimental observations. Additionally, whenever CT processes may be indicated (experimentally or computationally), the authors recommend comparing the data against either cam-QTP(01) or LC-ωHPBE. The cam-QTP(01) functional performed particularly well, thus making it an affordable candidate for potential screening studies. The initial experimental assignment of a CT emission process can now be better described as a local $\pi^*-\pi$ emission, similar to the other azaborine derivatives, that occurs from the charge-separated state. The separation of charge is created by a significant decrease in the pK_a of the nitro compounds in the ES and subsequent deprotonation during relaxation of the S_1 state; effectively, the nitro compounds appear to act as photoacids. Increased solvent stabilization of this charge-separated geometry explains the larger Stokes shift in more polar solvents.

ASSOCIATED CONTENT

Supporting Information

The Supporting Information is available free of charge at https://pubs.acs.org/doi/10.1021/acs.jpca.0c05765.

NTOs, pK_as, simulated spectra, tabulated data, and molecular coordinates (*XYZ*) (PDF)

AUTHOR INFORMATION

Corresponding Author

Charles Edwin Webster − *Department of Chemistry, Mississippi State University, Mississippi State, Mississippi 39762, United States;* orcid.org/0000-0002-6917-2957; Email: ewebster@chemistry.msstate.edu

Authors

Robert W. Lamb − *Department of Chemistry, Mississippi State University, Mississippi State, Mississippi 39762, United States;* orcid.org/0000-0001-6463-3809

Alan K. Schrock − *Department of Chemistry, University of West Florida, Pensacola, Florida 32514, United States*

Michael T. Huggins − *College of Science and Technology, Tarleton State University, Stephenville, Texas 76402, United States;* orcid.org/0000-0002-4429-8668

Complete contact information is available at: https://pubs.acs.org/10.1021/acs.jpca.0c05765

Author Contributions

The manuscript was written through contributions of all authors. All authors have given approval to the final version of the manuscript.

Funding

This work was supported by the National Science Foundation (CHE 1800201 and OIA 1539035), the High-Performance Computing Collaboratory (HPC^2), and the Mississippi Center for Supercomputing Research (MCSR).

Notes

The authors declare no competing financial interest.

ACKNOWLEDGMENTS

The authors would like to acknowledge Professor Steven Gwaltney for valuable discussions during this project, the National Science Foundation (CHE 1800201 and OIA 1539035) for funding, and the High-Performance Computing

Collaboratory (HPC^2) and the Mississippi Center for Supercomputing Research (MCSR) for computational resources.

REFERENCES

(1) Chinta, R. V. R. N.; Aradhyula, B. P. R.; Murali, A. C.; Venkatasubbaiah, K. Synthesis, photophysical and electrochemical properties of naphthaldimine based boron complexes. *J. Organomet. Chem.* **2019**, *891*, 20−27.

(2) Mula, S.; Leclerc, N.; Lévêque, P.; Retailleau, P.; Ulrich, G. Synthesis of Indolo[3,2-*b*]carbazole-Based Boron Complexes with Tunable Photophysical and Electrochemical Properties. *J. Org. Chem.* **2018**, *83*, 14406−14418.

(3) Frath, D.; Massue, J.; Ulrich, G.; Ziessel, R. Luminescent Materials: Locking π-Conjugated and Heterocyclic Ligands with Boron(III). *Angew. Chem., Int. Ed.* **2014**, *53*, 2290−2310.

(4) Wang, J.; Wu, Q.; Yu, C.; Wei, Y.; Mu, X.; Hao, E.; Jiao, L. Aromatic Ring Fused BOPHYs as Stable Red Fluorescent Dyes. *J. Org. Chem.* **2016**, *81*, 11316−11323.

(5) Saint-Louis, C. J.; Magill, L. L.; Wilson, J. A.; Schroeder, A. R.; Harrell, S. E.; Jackson, N. S.; Trindell, J. A.; Kim, S.; Fisch, A. R.; Munro, L.; Catalano, V. J.; Webster, C. E.; Vaughan, P. P.; Molek, K. S.; Schrock, A. K.; Huggins, M. T. The Synthesis and Characterization of Highly Fluorescent Polycyclic Azaborine Chromophores. *J. Org. Chem.* **2016**, *81*, 10955−10963.

(6) Wang, J.-Y.; Pei, J. BN-embedded aromatics for optoelectronic applications. *Chin. Chem. Lett.* **2016**, *27*, 1139−1146.

(7) Li, G.; Zhao, Y.; Li, J.; Cao, J.; Zhu, J.; Sun, X. W.; Zhang, Q. Synthesis, Characterization, Physical Properties, and OLED Application of Single BN-Fused Perylene Diimide. *J. Org. Chem.* **2015**, *80*, 196−203.

(8) Wang, X.-Y.; Lin, H.-R.; Lei, T.; Yang, D.-C.; Zhuang, F.-D.; Wang, J.-Y.; Yuan, S.-C.; Pei, J. Azaborine Compounds for Organic Field-Effect Transistors: Efficient Synthesis, Remarkable Stability, and BN Dipole Interactions. *Angew. Chem., Int. Ed.* **2013**, *52*, 3117−3120.

(9) Wang, X.-Y.; Zhuang, F.-D.; Wang, J.-Y.; Pei, J. Incorporation of polycyclic azaborine compounds into polythiophene-type conjugated polymers for organic field-effect transistors. *Chem. Commun.* **2015**, *51*, 17532−17535.

(10) Srivastava, A.; Santhibhushan, B.; Sharma, V.; Kaur, K.; Shahzad Khan, M.; Marathe, M.; De Sarkar, A.; Shahid Khan, M. Influence of Boron Substitution on Conductance of Pyridine- and Pentane-Based Molecular Single Electron Transistors: First-Principles Analysis. *J. Electron. Mater.* **2016**, *45*, 2233−2241.

(11) Saint-Louis, C. J.; Shavnore, R. N.; McClinton, C. D. C.; Wilson, J. A.; Magill, L. L.; Brown, B. M.; Lamb, R. W.; Webster, C. E.; Schrock, A. K.; Huggins, M. T. Synthesis, computational, and spectroscopic analysis of tunable highly fluorescent BN-1,2-azaborine derivatives containing the N-BOH moiety. *Org. Biomol. Chem.* **2017**, *15*, 10172−10183.

(12) Etienne, T.; Assfeld, X.; Monari, A. Toward a Quantitative Assessment of Electronic Transitions' Charge-Transfer Character. *J. Chem. Theory Comput.* **2014**, *10*, 3896−3905.

(13) Dreuw, A.; Weisman, J. L.; Head-Gordon, M. Long-range charge-transfer excited states in time-dependent density functional theory require non-local exchange. *J. Chem. Phys* **2003**, *119*, 2943−2946.

(14) Tozer, D. J. Relationship between long-range charge-transfer excitation energy error and integer discontinuity in Kohn−Sham theory. *J. Chem. Phys.* **2003**, *119*, 12697−12699.

(15) Peach, M. J. G.; Benfield, P.; Helgaker, T.; Tozer, D. J. Excitation energies in density functional theory: An evaluation and a diagnostic test. *J. Chem. Phys.* **2008**, *128*, No. 044118.

(16) Eriksen, J. J.; Sauer, S. P. A.; Mikkelsen, K. V.; Christiansen, O.; Jensen, H. J. A.; Kongsted, J. Failures of TDDFT in describing the lowest intramolecular charge-transfer excitation in *para*-nitroaniline. *Mol. Phys.* **2013**, *111*, 1235−1248.

(17) Le Guennic, B.; Jacquemin, D. Taking Up the Cyanine Challenge with Quantum Tools. *Acc. Chem. Res.* **2015**, *48*, 530−537.

(18) Chibani, S.; Laurent, A. D.; Le Guennic, B.; Jacquemin, D. Excited States of Ladder-Type π-Conjugated Dyes with a Joint SOS-CIS(D) and PCM-TD-DFT Approach. *J. Phys. Chem. A* **2015**, *119*, 5417−5425.

(19) Momeni, M. R.; Brown, A. Why Do TD-DFT Excitation Energies of BODIPY/Aza-BODIPY Families Largely Deviate from Experiment? Answers from Electron Correlated and Multireference Methods. *J. Chem. Theory Comput.* **2015**, *11*, 2619−2632.

(20) Fazen, P. J.; Burke, L. A. Theoretical Studies of Borazynes and Azaborines. *Inorg. Chem.* **2006**, *45*, 2494−2500.

(21) Mahapatra, A. K.; Maji, R.; Maiti, K.; Manna, S. K.; Mondal, S.; Das Mukhopadhyay, C.; Goswami, S.; Sarkar, D.; Mondal, T. K.; Quah, C. K.; Fun, H.-K. Synthesis and anion sensing properties of novel N,O-chelated perimidine−BF complex. *Sens. Actuators, B* **2015**, *207*, 878−886.

(22) Lee, C.; Yang, W.; Parr, R. G. Development of the Colle-Salvetti correlation-energy formula into a functional of the electron density. *Phys. Rev. B* **1988**, *37*, 785−789.

(23) Becke, A. D. Density-functional thermochemistry. III. The role of exact exchange. *J. Chem. Phys.* **1993**, *98*, 5648−5652.

(24) Perdew, J. P.; Burke, K.; Ernzerhof, M. Generalized Gradient Approximation Made Simple. *Phys. Rev. Lett.* **1996**, *77*, 3865.

(25) Perdew, J. P.; Burke, K.; Ernzerhof, M. Generalized Gradient Approximation Made Simple. *Phys. Rev. Lett.* **1996**, *77*, 3865−3868.

(26) Adamo, C.; Barone, V. Toward reliable density functional methods without adjustable parameters: The PBE0 model. *J. Chem. Phys.* **1999**, *110*, 6158−6170.

(27) Grimme, S. Semiempirical GGA-type density functional constructed with a long-range dispersion correction. *J. Comput. Chem.* **2006**, *27*, 1787−1799.

(28) Jin, Y.; Bartlett, R. J. The QTP family of consistent functionals and potentials in Kohn-Sham density functional theory. *J. Chem. Phys.* **2016**, *145*, No. 034107.

(29) Henderson, T. M.; Izmaylov, A. F.; Scalmani, G.; Scuseria, G. E. Can short-range hybrids describe long-range-dependent properties? *J. Chem. Phys.* **2009**, *131*, No. 044108.

(30) Chai, J.-D.; Head-Gordon, M. Long-range corrected hybrid density functionals with damped atom-atom dispersion corrections. *Phys. Chem. Chem. Phys.* **2008**, *10*, 6615−6620.

(31) Frisch, M. J.; Trucks, G. W.; Schlegel, H. B.; Scuseria, G. E.; Robb, M. A.; Cheeseman, J. R.; Scalmani, G.; Barone, V.; Mennucci, B.; Petersson, G. A.; Nakatsuji, H.; Caricato, M.; Li, X.; Hratchian, H. P.; Izmaylov, A. F.; Bloino, J.; Zheng, G.; Sonnenberg, J. L.; Hada, M.; Ehara, M.; Toyota, K.; Fukuda, R.; Hasegawa, J.; Ishida, M.; Nakajima, T.; Honda, Y.; Kitao, O.; Nakai, H.; Vreven, T.; Montgomery, J. A., Jr.; Peralta, J. E.; Ogliaro, F.; Bearpark, M. J.; Heyd, J.; Brothers, E. N.; Kudin, K. N.; Staroverov, V. N.; Kobayashi, R.; Normand, J.; Raghavachari, K.; Rendell, A. P.; Burant, J. C.; Iyengar, S. S.; Tomasi, J.; Cossi, M.; Rega, N.; Millam, N. J.; Klene, M.; Knox, J. E.; Cross, J. B.; Bakken, V.; Adamo, C.; Jaramillo, J.; Gomperts, R.; Stratmann, R. E.; Yazyev, O.; Austin, A. J.; Cammi, R.; Pomelli, C.; Ochterski, J. W.; Martin, R. L.; Morokuma, K.; Zakrzewski, V. G.; Voth, G. A.; Salvador, P.; Dannenberg, J. J.; Dapprich, S.; Daniels, A. D.; Farkas, Ö.; Foresman, J. B.; Ortiz, J. V.; Cioslowski, J.; Fox, D. J. *Gaussian 09*; Gaussian, Inc.: Wallingford, CT USA, 2009

(32) Frisch, M. J.; Trucks, G. W.; Schlegel, H. B.; Scuseria, G. E.; Robb, M. A.; Cheeseman, J. R.; Scalmani, G.; Barone, V.; Petersson, G. A.; Nakatsuji, H.; Li, X.; Caricato, M.; Marenich, A. V.; Bloino, J.; Janesko, B. G.; Gomperts, R.; Mennucci, B.; Hratchian, H. P.; Ortiz, J. V.; Izmaylov, A. F.; Sonnenberg, J. L.; Williams-Young, D.; Ding, F.; Lipparini, F.; Egidi, F.; Goings, J.; Peng, B.; Petrone, A.; Henderson, T.; Ranasinghe, D.; Zakrzewski, V. G.; Gao, J.; Rega, N.; Zheng, G.; Liang, W.; Hada, M.; Ehara, M.; Toyota, K.; Fukuda, R.; Hasegawa, J.; Ishida, M.; Nakajima, T.; Honda, Y.; Kitao, O.; Nakai, H.; Vreven, T.; Throssell, K.; Montgomery, J. A., Jr.; Peralta, J. E.; Ogliaro, F.; Bearpark, M. J.; Heyd, J. J.; Brothers, E. N.; Kudin, K. N.; Staroverov, V. N.; Keith, T. A.; Kobayashi, R.; Normand, J.; Raghavachari, K.; Rendell, A. P.; Burant, J. C.; Iyengar, S. S.; Tomasi, J.; Cossi, M.;

Millam, J. M.; Klene, M.; Adamo, C.; Cammi, R.; Ochterski, J. W.; Martin, R. L.; Morokuma, K.; Farkas, O.; Foresman, J. B.; Fox, D. J. *Gaussian 16 A.03*; Gaussian, Inc.: Wallingford, CT, USA., 2016

(33) Shao, Y.; Gan, Z.; Epifanovsky, E.; Gilbert, A. T. B.; Wormit, M.; Kussmann, J.; Lange, A. W.; Behn, A.; Deng, J.; Feng, X.; Ghosh, D.; Goldey, M.; Horn, P. R.; Jacobson, L. D.; Kaliman, I.; Khaliullin, R. Z.; Kuś, T.; Landau, A.; Liu, J.; Proynov, E. I.; Rhee, Y. M.; Richard, R. M.; Rohrdanz, M. A.; Steele, R. P.; Sundstrom, E. J.; Woodcock, H. L., III; Zimmerman, P. M.; Zuev, D.; Albrecht, B.; Alguire, E.; Austin, B.; Beran, G. J. O.; Bernard, Y. A.; Berquist, E.; Brandhorst, K.; Bravaya, K. B.; Brown, S. T.; Casanova, D.; Chang, C.-M.; Chen, Y.; Chien, S. H.; Closser, K. D.; Crittenden, D. L.; Diedenhofen, M.; DiStasio, R. A., Jr.; Do, H.; Dutoi, A. D.; Edgar, R. G.; Fatehi, S.; Fusti-Molnar, L.; Ghysels, A.; Golubeva-Zadorozhnaya, A.; Gomes, J.; Hanson-Heine, M. W. D.; Harbach, P. H. P.; Hauser, A. W.; Hohenstein, E. G.; Holden, Z. C.; Jagau, T.-C.; Ji, H.; Kaduk, B.; Khistyaev, K.; Kim, J.; Kim, J.; King, R. A.; Klunzinger, P.; Kosenkov, D.; Kowalczyk, T.; Krauter, C. M.; Lao, K. U.; Laurent, A. D.; Lawler, K. V.; Levchenko, S. V.; Lin, C. Y.; Liu, F.; Livshits, E.; Lochan, R. C.; Luenser, A.; Manohar, P.; Manzer, S. F.; Mao, S.-P.; Mardirossian, N.; Marenich, A. V.; Maurer, S. A.; Mayhall, N. J.; Neuscamman, E.; Oana, C. M.; Olivares-Amaya, R.; O'Neill, D. P.; Parkhill, J. A.; Perrine, T. M.; Peverati, R.; Prociuk, A.; Rehn, D. R.; Rosta, E.; Russ, N. J.; Sharada, S. M.; Sharma, S.; Small, D. W.; Sodt, A.; Stein, T.; Stück, D.; Su, Y.-C.; Thom, A. J. W.; Tsuchimochi, T.; Vanovschi, V.; Vogt, L.; Vydrov, O.; Wang, T.; Watson, M. A.; Wenzel, J.; White, A.; Williams, C. F.; Yang, J.; Yeganeh, S.; Yost, S. R.; You, Z.-Q.; Zhang, I. Y.; Zhang, X.; Zhao, Y.; Brooks, B. R.; Chan, G. K. L.; Chipman, D. M.; Cramer, C. J.; Goddard, W. A., III; Gordon, M. S.; Hehre, W. J.; Klamt, A.; Schaefer, H. F., III; Schmidt, M. W.; Sherrill, C. D.; Truhlar, D. G.; Warshel, A.; Xu, X.; Aspuru-Guzik, A.; Baer, R.; Bell, A. T.; Besley, N. A.; Chai, J.-D.; Dreuw, A.; Dunietz, B. D.; Furlani, T. R.; Gwaltney, S. R.; Hsu, C.-P.; Jung, Y.; Kong, J.; Lambrecht, D. S.; Liang, W.; Ochsenfeld, C.; Rassolov, V. A.; Slipchenko, L. V.; Subotnik, J. E.; Van Voorhis, T.; Herbert, J. M.; Krylov, A. I.; Gill, P. M. W.; Head-Gordon, M. Advances in molecular quantum chemistry contained in the Q-Chem 4 program package. *Mol. Phys.* **2015**, *113*, 184−215.

(34) McLean, A. D.; Chandler, G. S. Contracted Gaussian basis sets for molecular calculations. I. Second row atoms, Z=11−18. *J. Chem. Phys.* **1980**, *72*, 5639−5648.

(35) Petersson, G. A.; Al-Laham, M. A. A complete basis set model chemistry. II. Open-shell systems and the total energies of the first-row atoms. *J. Chem. Phys.* **1991**, *94*, 6081−6090.

(36) Wadt, W. R.; Hay, P. J. Ab initio effective core potentials for molecular calculations. Potentials for main group elements Na to Bi. *J. Chem. Phys.* **1985**, *82*, 284−298.

(37) Check, C. E.; Faust, T. O.; Bailey, J. M.; Wright, B. J.; Gilbert, T. M.; Sunderlin, L. S. Addition of Polarization and Diffuse Functions to the LANL2DZ Basis Set for P-Block Elements. *J. Phys. Chem. A* **2001**, *105*, 8111−8116.

(38) Peterson, K. A.; Figgen, D.; Goll, E.; Stoll, H.; Dolg, M. Systematically convergent basis sets with relativistic pseudopotentials. II. Small-core pseudopotentials and correlation consistent basis sets for the post-d group 16-18 elements. *J. Chem. Phys.* **2003**, *119*, 11113−11123.

(39) Marenich, A. V.; Cramer, C. J.; Truhlar, D. G. Universal Solvation Model Based on Solute Electron Density and on a Continuum Model of the Solvent Defined by the Bulk Dielectric Constant and Atomic Surface Tensions. *J. Phys. Chem. B* **2009**, *113*, 6378−6396.

(40) Dunnig, T. H., Jr. Gaussian basis sets for use in correlated molecular calculations. I. The atoms boron through neon and hydrogen. *J. Chem. Phys.* **1989**, *90*, 1007−1023.

(41) Papajak, E.; Zheng, J.; Xu, X.; Leverentz, H. R.; Truhlar, D. G. Perspectives on Basis Sets Beautiful: Seasonal Plantings of Diffuse Basis Functions. *J. Chem. Theory Comput.* **2011**, *7*, 3027−3034.

(42) Vetterling, W. T.; Press, W. H. *Numerical recipes in FORTRAN : the art of scientific computing*; 2nd Ed.; Cambridge University Press: Cambridge England, New York, NY, USA., 1992

(43) Improta, R.; Barone, V.; Scalmani, G.; Frisch, M. J. A state-specific polarizable continuum model time dependent density functional theory method for excited state calculations in solution. *J. Chem. Phys.* **2006**, *125*, No. 054103.

(44) Improta, R. The excited states of π-stacked 9-methyladenine oligomers: a TD-DFT study in aqueous solution. *Phys. Chem. Chem. Phys.* **2008**, *10*, 2656.

(45) Barone, V.; Bloino, J.; Biczysko, M.; Santoro, F. Fully Integrated Approach to Compute Vibrationally Resolved Optical Spectra: From Small Molecules to Macrosystems. *J. Chem. Theory Comput.* **2009**, *5*, 540−554.

(46) Santoro, F.; Lami, A.; Improta, R.; Bloino, J.; Barone, V. Effective method for the computation of optical spectra of large molecules at finite temperature including the Duschinsky and Herzberg−Teller effect: The Q_x band of porphyrin as a case study. *J. Chem. Phys.* **2008**, *128*, 224311.

(47) Santoro, F.; Improta, R.; Lami, A.; Bloino, J.; Barone, V. Effective method to compute Franck-Condon integrals for optical spectra of large molecules in solution. *J. Chem. Phys.* **2007**, *126*, No. 084509.

(48) Santoro, F.; Lami, A.; Improta, R.; Barone, V. Effective method to compute vibrationally resolved optical spectra of large molecules at finite temperature in the gas phase and in solution. *J. Chem. Phys.* **2007**, *126*, 184102.

(49) Etienne, T.; Assfeld, X.; Monari, A. New Insight into the Topology of Excited States through Detachment/Attachment Density Matrices-Based Centroids of Charge. *J. Chem. Theory Comput.* **2014**, *10*, 3906−3914.

(50) Etienne, T. Probing the Locality of Excited States with Linear Algebra. *J. Chem. Theory Comput.* **2015**, *11*, 1692−1699.

(51) Marriott, K.-S. C.; Morrison, A. Z.; Moore, M.; Olubajo, O.; Stewart, L. E. Synthesis of *N*-phenyl-*N*-(3-(piperidin-1-yl)propyl)-benzofuran-2-carboxamides as new selective ligands for sigma receptors. *Bioorg. Med. Chem.* **2012**, *20*, 6856−6861.

(52) Loos, P.-F.; Lipparini, F.; Boggio-Pasqua, M.; Scemama, A.; Jacquemin, D. A Mountaineering Strategy to Excited States: Highly Accurate Energies and Benchmarks for Medium Sized Molecules. *J. Chem. Theory Comput.* **2020**, *16*, 1711−1741.

(53) Kánnár, D.; Szalay, P. G. Benchmarking Coupled Cluster Methods on Valence Singlet Excited States. *J. Chem. Theory Comput.* **2014**, *10*, 3757−3765.

(54) Schreiber, M.; Silva-Junior, M. R.; Sauer, S. P. A.; Thiel, W. Benchmarks for electronically excited states: CASPT2, CC2, CCSD, and CC3. *J. Chem. Phys.* **2008**, *128*, 134110.

(55) Send, R.; Valsson, O.; Filippi, C. Electronic Excitations of Simple Cyanine Dyes: Reconciling Density Functional and Wave Function Methods. *J. Chem. Theory Comput.* **2011**, *7*, 444−455.

(56) Pinto da Silva, L.; Green, O.; Gajst, O.; Simkovitch, R.; Shabat, D.; Esteves da Silva, J. C. G.; Huppert, D. Excited-State Proton Transfer of Phenol Cyanine Picolinium Photoacid. *ACS Omega* **2018**, *3*, 2058−2073.

(57) Bochevarov, A. D.; Harder, E.; Hughes, T. F.; Greenwood, J. R.; Braden, D. A.; Philipp, D. M.; Rinaldo, D.; Halls, M. D.; Zhang, J.; Friesner, R. A. Jaguar: A high-performance quantum chemistry software program with strengths in life and materials sciences. *Int. J. Quantum Chem.* **2013**, *113*, 2110−2142.

https://dx.doi.org/10.1021/acs.jpca.0c05765
J. Phys. Chem. A 2021, 125, 3−12